Mon. Not. R. Astron. Soc. **000**, 1–6 (2002) Printed 28 March 2017 (MN LATEX style file v2.2)

MADX

S.J. Maddox[1] ⋆, L. Dunne[1]

ABSTRACT

We describe a simple technique for detecting sources in multiband imaging. The method is to filter the individual bands by the corresponding point-spread function (PSF), and for the inverse variance weighted sum of the individual bands. Peaks in this combined image are then used as the best estimates of the positions of sources in the data. The fluxes for each source are then estimated from the individual band images.

We generate a simulated 4×4 degrees patch of sky in 110, 170, 250, 250 and 500 micron bands, using source counts from a simple model which matches the observed sub-mm counts, and Cosmic Infrared Background. The source positions were clustered like normal galaxies. The simulated sky is blurred by realistic PSF and has Gaussian noise added. We then use our method to find sources in the noisy blurred data and compare to the input source list. We also use Sextractor to identify sources and compare the completeness reliability of our method to this approach. We find that the multiband approach allows reliable source detection almost a factor 2 lower in flux, and that the positional reliability is sources is greatly improved for the longer wavelength bands.

Key words:

1 INTRODUCTION

There are many well-known algorithms to detect sources in imaging data. For an isolated point source, with a uniform background and simple Gaussian noise, it is straightforward to show that the optimal way to detect it is to filter the data with the point-spread function and find the peak in the filtered map. The value of the peak is equivalent to a least squares fit of the psf to the data at the position of the peak, and so in some sense is the optimal flux estimate of the source.

It is often the case that data are available in multiple wavebands, and band-matched source catalogues are required. This paper describes a simple method to combine multiwavelength data in a way that enhances the source detection and automatically produces a band-matched catalogue. This method has been used to find sources in data for the Herschel ATLAS programme (Eales et al. (2010)), but it could easily be applied more widely.

Each section in this paper describes a step in the method: estimate and subtract a non-uniform background; filter the map for each waveband; combine the wavebands; detect sources and determine their positions; and estimate their fluxes. The final two sections of the paper describes some simulations which are used to demonstrate the algorithm, both in a simple single source case and more realistic simulations representing the sub-mm sky as seen by the Herschel satellite.

⋆ E-mail: steve.maddox@nottingham.ac.uk

2 BACKGROUND ESTIMATION

The first step in detecting sources is to subtract the background, which may be spatially varying. In general it is impossible to differentiate between multiple confused sources and a smoothly varying component, but in either case, it is necessary to remove the contribution of the background flux from an individual source. So, we need to determine the local background around at any position in the map. We have done this by splitting the map into blocks of pixels corresponding to $\sim 10 \times FWHM$, and constructing a histogram of pixel values for each block. We then fit a Gaussian to the peak of the histogram, and compare to the median value. If the peak is more than one-σ from the median, the fit is flagged as unreliable, and we use the median. Near the edges of the map, there may be only a small number of pixels contributing to a block. If there are less than 20 pixels in a block, the background is not estimated from the local pixels, but is set to the final mean background from the whole map.

The fitted peak of the histogram is very insensitive to a small number of bright sources in the block. As a simple test we made a set of 1000 realizations of a model with a background of 10mJy with Gaussian random noise with an rms of 6mJy, and put a single 1Jy Gaussian source in the middle. The resulting histogram for a single realization is shown in Figure 1. The mean of the block is 42mJy, and so would give an error of 32 mJy if it were used as the background estimate. The median is more robust, leading to an error of 1mJy, and the peak fit is biased by only 0.3 mJy. It is worth noting that simple Fourier filter methods, such as the Weiner filter, are intrinsically linear, and so are approximately equivalent to using the local mean value as the background estimate. This means that they can be significantly biased around bright sources.

© 2002 RAS

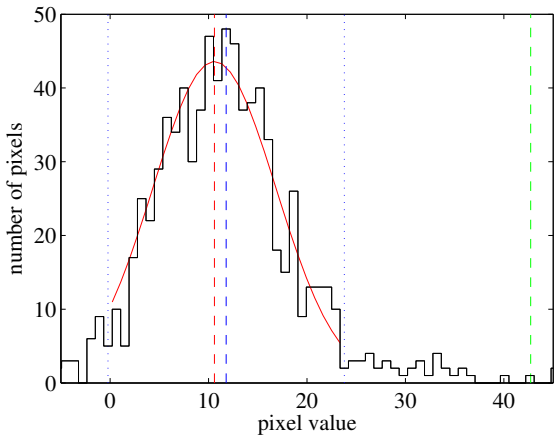

Figure 1. Simulated histogram of pixel values in a background block. The model has a true background of 10mJy with 6mJy Gaussian noise and a single 1Jy source in the centre. The red line is the best fit Gaussian. The fitted peak is is 10.3mJy (red dashed line), the median is 11.3mJy (blue dashed line), and the mean is 42mJy (green dashed line). The dotted blue lines are the $\pm 2\sigma$ from the median.

The background at each pixel is then estimated using a bicubic interpolation between the coarse grid of backgrounds, and subtracted from the data.

This approach to background estimateion is similar in principle to the `nebuliser` algorithm of Irwin (??)

???

3 FILTERING

Typically image data is sampled finely enough that point sources are sampled by 2 or 3 pixels in each direction. This means that the flux is spread over several pixels, and the optimal estimate of the source flux is given by a weighted sum over pixels. Convolving the map by the right filter function will maximize the signal-to-noise for detecting sources, and estimating their flux. For an isolated source on a uniform background with Gaussian errors, the optimal filter is the point spread function (PSF), weighted by the inverse of the local inverse if the variance is spatially varying. In general the optimal filter may be different from the PSF. For example, when the source density is high, confusion noise is important, and the optimal filter is narrower than the PSF. The optimal filter can be estimated using a Wiener filter approach that includes confusion noise (see Chapmin et al 2011). The noise-weighted filtered map, F, is given by

$$F = \frac{(DW) \otimes P}{W \otimes PQ}, \quad (1)$$

where D is the background subtracted data in each pixel, the weight $W = 1/\mathrm{var}(D)$ is the inverse of the variance of each pixel, P is the PSF, and $\otimes$ represents the convolution operator On the assumption that the instrumental noise on each pixel in the unfiltered map is uncorrelated, the variance of each pixel in the filtered map is given by

$$V = \frac{1}{W \otimes PQ}, \quad (2)$$

This is a simple generalization of the PSF-filtering derived by Serjeant et al (Serjeant et al 2003).

The filtered map gives the minimum χ^2 estimate of the flux that a source would have at any given pixel in the map. Standard FFT routines allow easy calculation of the convolved maps at integer pixel positions, but in practice, sources are not necessarily centered on pixels. In order to find the best flux estimates, we need to allow for sub-pixel positioning. Without this, the fluxes will be significantly underestimated, particularly when a source lies at the edge of a pixel. Our approach to solving this problem is discussed in Section 5.

4 COMBINING WAVEBANDS

The filtered maps provide estimates of source flux and uncertainty at any position, but they can also be linked to the likelihood ratio of there being a source at each position rather than background. Assuming uncorrelated Gaussian errors, the probability of a part of the map being simply background is

$$P_b = \prod \exp\left(-\frac{1}{2} d_i^2/\sigma_i^2\right),$$

and the corresponding probability of being a point source is

$$P_s = \prod \exp\left(-\frac{1}{2} (d_i - s_i)^2/\sigma_i^2\right),$$

where s_i is the flux distribution of the best-fit point source, $s_i = FP_i$. The minimum χ^2 value of the source flux is F, given by Eqn1, and the value of χ^2 at the minimum is $\sum (d_i^2/\sigma_i^2) - F^2/V^2$. This means that maximum log-likelihood ratio of being a source compared to being background is simply

$$F^2/2V^2.$$

This idea can be extended to include any other wavebands that are available. If we know the observed spectral energy distribution (SED), $S(\lambda)$ of a source then we can calculate the flux in a band k with response $R_k(\lambda)$,

$$F_k = \frac{\int S(\lambda) R_k(\lambda) d\lambda}{\int (R_k(\lambda) d\lambda}$$

Given a set of filters pass-bands, we can calculate the flux in each band. If we write the normalized SED $S_0(\lambda) = S(\lambda)/\int S(\lambda) d\lambda$, then the SED of the source is $AS_0(\lambda)$, where $A = \int S(\lambda) d\lambda$. We can also write the broad-band flux in each band as AS_{0k}, where

$$S_{0k} = \frac{\int S_0(\lambda) R_k(\lambda) d\lambda}{\int (R_k(\lambda) d\lambda}$$

The values of S_{0k} for each band are the expected fluxes for a source with the given SED and unit bolometric flux. The expected flux for any particular source will be AS_{0k}. Each individual band gives an independent estimate of A, from the filtered map in that band. In order to combine the maps, we need to have the independent estimates at exactly the same position. As discussed in the previous section, it is best to use a bicubic interpolation to estimate the source flux at non-integer positions. If we interpolate the lower resolution maps to the pixels of the highest resolution map, then we can combine them to obtain the minimum variance estimate of A at any position in the maps. For waveband k the estimate of A at position x is $A_k = F_k(x)/S_{0k}$, and the variance is $\sigma_k^2 = V_k(x)/S_{0k}^2$. The minimum variance estimate of A is then given by

$$A_{tot} = \sum_k S_{0k} \frac{F_k}{V_k} \Big/ \sum_k \frac{S_{0k}^2}{V_k}$$

Note that this includes the factor S_{0k} as part of the weight given to the waveband k so that the prior expected SED acts as a weighting term for each band as well as the inverse variance weighting. This makes intuitive sense: if a source's flux is expected to peak in a particular band, we should give that band the most weight in determining the position of the source; if a source has a flat spectrum, so that the flux is equal in all bands, then all bands are given equal weight.

The uncertainty on A_{tot} is given by

$$\sigma_A^2 = \sum_k \frac{S_{0k}^2}{V_k},$$

so the significance of a source detection at any position is A_{tot}/σ_A. As for a single band, we can now find the most likely position of the source as the peak of the combined significance map. For the whole map, we first identify all local peaks in the significance map, and retain those that are $\gtrsim 2\sigma$ as potential sources. In principle we could retain all peaks, but rejecting the low-significance peaks gives a great computational efficiency saving. Next, a variance weighted least-squares fit of a Gaussian is performed on the 5×5 pixels around each peak. The position of the peak is allowed to vary freely, and is not constrained to be at integer pixel positions. Since the position can be a non-integer pixel, we fit to the peak to find the best position at the sub-pixel level. We fit only to pixels near the peak to minimize the effects of confusion from other nearby sources. Since the individual maps have been filtered, the peak pixels already include data from the surrounding raw pixels in combined in an optimal way; the peak fitting is solely to find the position at the sub-pixel level.

In order to estimate the flux in each band, we go back to the filtered maps, and interpolate to find the value of the map at the position of the peak in the combined map. If there are sources that are close together, this simple approach will 'double-count' flux, assigning it to both source in a pair. A simple way to avoid this is to sort the sources in order of flux and then subtract off the filtered PSF scaled by the relevant flux for each source in sequence of decreasing flux. This is rather like a single-pass 'clean'. In principle, the procedure could be iterated to a stable solution, but in practice the difficult cases are blends of sources that require a more sophisticated de-blending technique to improve the flux estimates. in future releases we plan to implement multi-source fitting to blended sources.

5 SUB-PIXEL SUBTLETIES

The above anaylsis ignires the complication that our data typically sample the sky with only 2 or 3 pixels across the FWHM of the psf. In order to obtain the most accurate estimates of flux and positions, we need to consider the true flux distribution within each pixel. The positions are estimated by fitting a Gaussian to central five-by-five grid of pixels for each detected peak in the map. This provides our best estimate of the source position, typically to better than 1/10 of a pixel.

The obvious way to improve on integer positions is to interpolate between integer pixels. A bilinear interpolation does not remove the bias, as can be seen by considering a source that is exactly half way between two pixels; each pixel will have the same value

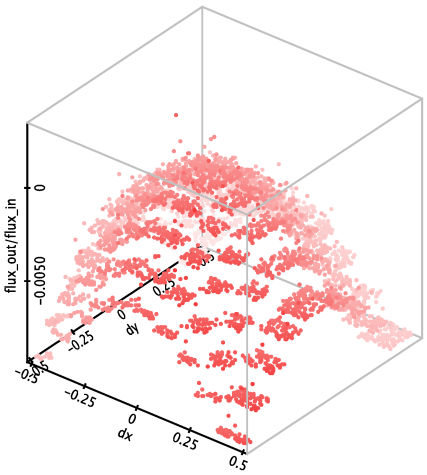

Figure 2. Fractional flux errors as a function of the precise source position within a pixel. The maximum error is $\sim 0.75\%$ for a source in the corner of 4 pixels. Sources were placed in the simulations at 0.1 pixel positions, which creates the 0.1 pixel patches.

that less than the true peak value, so the interpolated value will also be biased low. A bicubic interpolation allows the interpolated value to be higher than either individual pixel, and so gives a better flux estimate.

The average flux error expected from simply using the value of the peak pixel can easily calculated, but there will still be a larger variance introduced by the sub-pixel position of different sources. Using the bicubic interpolation reduces this scatter and improves the accuracy of the flux measurements.

When the psf is sampled into coarse pixels, the value of the peak pixel is averaged over the whole area of the central pixel, and so is suppressed relative to the true psf. For a psf tha is close to a gaussian with 3 pixels across the FWHM, this suppression is typically 5%. If we use the pixelated psf (the Point Response Function - or PRF) when filtering the data, this filtered data is boosted by the suppression factor, and so a source that is centred in a pixel retuns the correct flux. When a source of not centred in a pixel, the peak pixel value is supressed more than for a centred source.

To estimate the flux of the source, we use a bi-cubic interpolation to find the flux at the source position using the pixels from the filtered maps. If the source position lies at the boundary between two pixels, the peak pixel value is suppressed relative to the peak of the pixel-centred psf. The bicubic interpolation means that the estimated flux will be higher than the pixel values, but still a slight underestimate of the actual peak. As seen in Figure 2 the error is largest for a source at the corner of 4 pixels when the flux is underestimated by $\sim 0.75\%$.

6 TESTS OF THE METHOD

As a simple test of the source detection we generated maps in 3 far–infrared and submillimetre bands (250, 350 and 500 μm) each map containing isolated sources on a grid of positions.

The sources are assigned random positions near the grid centres, so that the pixels sample the psf with random offsets from the pixel centres. Each source is given a 250 μm flux between 1mJy and 1Jy, uniformly spaced in log flux. The 350 μm and 500 μm fluxes for each source are then assigned so that the SED matches a modified black body with β chosen from a uniform random distribution

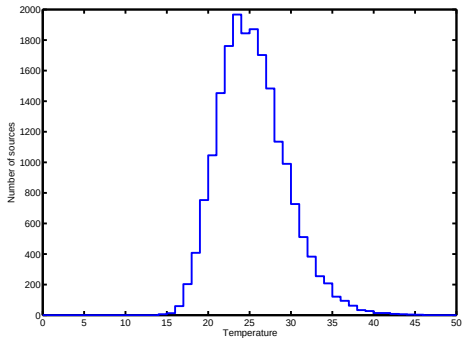

Figure 3. The temperature distribution of simulated sources.

between 1 and 2, and temperature, T, randomly chosen from a log-normal distribution centred on $T = 25$K, and ranging from 15K to 40K, as shown in Fig 3. This distribution roughly matches the SEDs of low-redshift galaxies seen in the Herschel-ATLAS survey (Smith et al 2012). To represent higher redshift galaxies, which appear much redder, we set $f_{350} = 2f_{250}$ and $f_{500} = 3f_{500}$. This matches the typical FIR colours for a z=4 galaxy.

We also added a galactic background by taking the SFD 100 μm and temperature maps and scaling the 100 μm emission to the relevant wavelength using a modified black-body. The resolution of the SFD maps is several arcminutes, and so does not contain small-scale structure in the cirrus background. The HATLAS data show that in some patches of sky there is strong cirrus emission with significant structure on sub-arcminute scales, but in most areas, the emission is relatively smooth. Our simulated background is a reasonable approximation for most of the sky, but will be somewhat easier to subtract than the areas where the true cirrus is particularly strong and structured.

Finally we add Gaussian noise to the maps. The standard deviation is varied by $\sqrt{N_{\rm passes}}$, where $N_{\rm passes}$ is the number of passes contributing to a pixel in a typical coverage map for the HATLAS survey data.

We then run MADX on the simulated maps to detect the input sources and measure their position and fluxes. A simple positional match allows us to associate the detected sources to the to the corresponding input sources, and so calculate the errors in position and fluxes. Since we put the sources on a randomized grid, there is no possibility of confusing one source with another. We used two different priors: first just using only the 250 μm band for the detection (weights 1,0,0); and second, equally weighting each band (weights 1,1,1). For each run, we measure the completeness by simply counting the fraction of input sources that are detected as a function of flux. Figure 4 shows the completeness as a function of the signal to noise in the 250 μm band.

It is clear that including information from all three bands significantly improves the completeness of the resulting catalogue. For sources with a red SED the gain is a factor 3 in signal-to-noise in the 250 μm band.

Next we compare the measured positions to the input positions. It may be thought that including data from lower resolution bands would increase the positional errors, but by using the correct weighting between the bands, the extra information actually improves the positional accuracy. This can be seen in Fig 5, which shows the rms position error in ra and dec as a function of signal-to-noise.

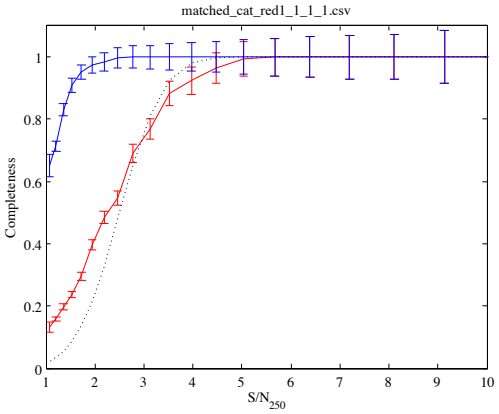

(a)

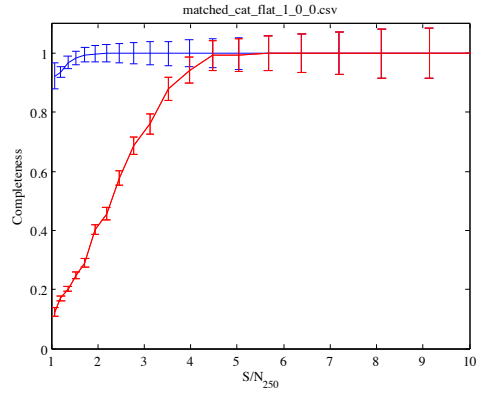

(b)

Figure 4.

Finally we compare the measured and input fluxes for the sources, in terms of both random and systematic errors. We compute the rms deviation of between the measured and input 250 μm flux as a function of the expected noise given the input Gaussian errors per pixel. As shown in Fig 6, the random errors match the input gaussian error for fainter sources. For brighter sources the fractional errors from the sub-pixel positioning begin to dominate, and the measured errors are larger than the Gaussian errors. The choice of prior makes little difference in the errors on the flux measurements, as the errors are dominated by the pixel errors on the map for each band. The exception is for faint 250 μm fluxes and the 250 μm only prior. The measured standard deviation for these sources is biased low because many sources with negative noise values fall below the detection threshold, and so do not contribute to the measured standard deviation, leading to an artificially low estimated noise. Using the flat prior mitigates this problem and the measured noise continues to match the expected noise to the lowest fluxes. The random noise on the 350 μm fluxes also match the expected noise. For the 500 μm band, the measured errors are 10% higher than expected

Fig 7 shows the mean ratio of measured to input flux as a function of signal to noise. At high signal to noise there is a small underestimate of flux due the peak pixelization issues discussed in section 5. For fainter sources near the detection limit, there is a systematic bias to higher fluxes (flux boosting). This is related to Eddington/Malmquist bias from when selecting only sources above a signal-to-noise threshold: faint sources with negative errors are not retained in the catalogue, whereas those with positive errors are detected to a fainter level. The precise form of the boosting depends

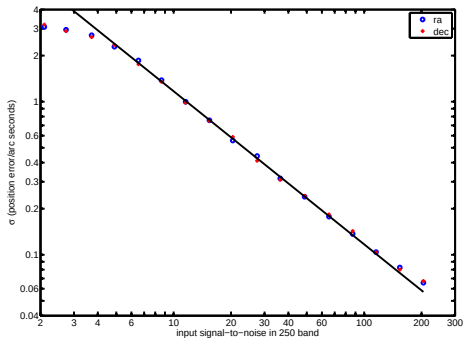

(a)

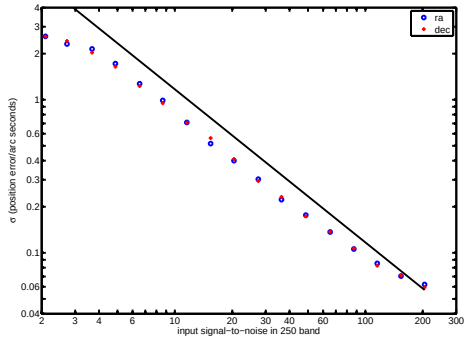

(b)

Figure 5. The measured positional errors of simulated sources plotted as a function of signal-to-noise in the 250 μm band. The standard deviation of the errors in ra are shown as blue circles, and in dec shown as red crosses. Panel (a) shows the measurements using only the 250 band to detect sources and measure their positions. Panel (b) shows the measurements using the flat-prior detection. The black line in both panels shows the variation expected from the theoretical analysis of Ivison (2007).

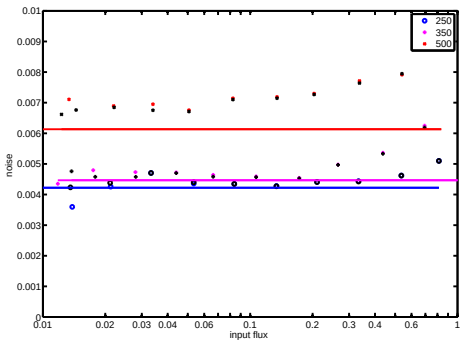

Figure 6. The measured signal to noise for each band measured as a function of input signal-to-noise in the 250 band. The expected The flat-prior and 250 only detection choice makes little difference in the resulting flux errors.

on the distribution of true source fluxes, as well as the measurement errors. For the simulations used here we chose to distribute sources uniformly in log flux, and so they do not match real source flux distributions, even though the colours are realistic. Hence we cannot use them to estimate the boosting as a function of flux for real data. Valiente et al (2016) a created realistic simulations and used them to estimate both completeness and boosting correction factors that apply to real data.

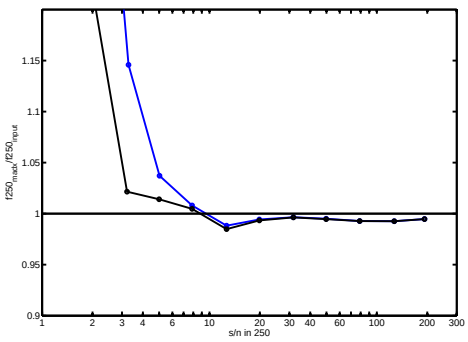

(a)

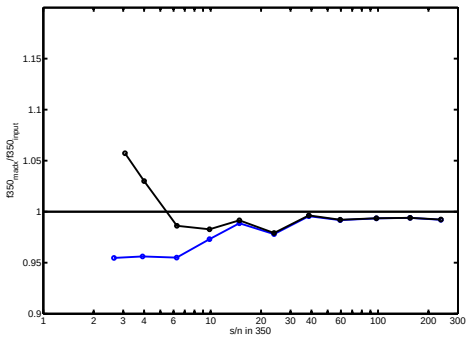

(b)

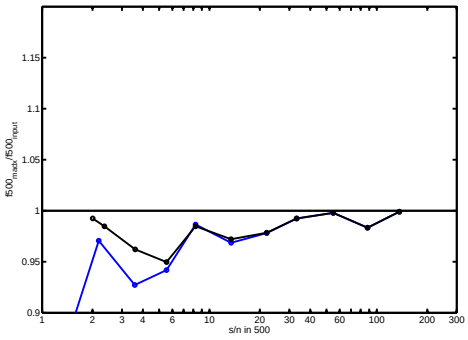

(c)

Figure 7. The ratio of mean measured flux compared to the mean input flux as a function of input signal to noise for two source detection priors. The blue line uses only the 250 band, and the black line uses a flat prior. Panel (a),(b) and (c) shows the results for the 250 μm , 350 μm and 500 μm fluxes respectively. Using the flat prior reduces the boosting effect at fainter fluxes.

For the other two bands, there is a similar small bias at high signal to noise, caused by peak pixelization effects. For fainter sources, there is a larger negative bias which is caused by positional errors, which mean that the local peak is missed and the flux estimate is systematically too low.

REFERENCES

Bertin, E., & Arnouts, S. 1996, AAPS, 117, 393
Clements, D. L., et al. 2010, A&A, in press, arXiv:1005.2409
Driver, S.P., et al., 2009, Astron. Geophys., 50, 5.12
Dunne, L., Eales, S. A., Edmunds, M., Ivison, R., Alexander, P., & Clements, D. L. 2000, MNRAS, 315, 115
Dye, S., et al., 2009 ApJ., 703, 285
Eales, S., et al. 2010, PASP, 122, 499

Griffin et al. 2010 A&A this issue.
Ibar, E., 2010, MNRAS, submitted
Ivison, R. J., et al. 2007, MNRAS, 380, 199
Maddox, S. J., et al. 2010, A&A, in press, arXiv:1005.2406
Negrello, M., Perrotta, F., González-Nuevo, J., Silva, L., de Zotti, G., Granato, G. L., Baccigalupi, C., & Danese, L. 2007, MNRAS, 377, 1557
Ott, S. 2010, in ASP Conference Series, Astronomical Data Analysis Software and Systems XIX, Y. Mizumoto, K.-I. Morita, and M. Ohishi, eds., in press
Pascale, E., et al, 2010, MNRAS, submitted
Pilbratt, G. L., et al. A&A in press, arXiv:1005.5331
Poglitsch, A., et al. 2010 A&A, in press, arXiv:1005.1487
Rigby, E.E, et al., MNRAS.
Rowan-Robinson, M. 2001, in IAU Symp. 204, The Extragalactic Infrared Background and its Cosmological Implications, ed. M. Harwit & M. G. Hauser (Dordrecht: Kluwer), 265
Schlegel, D. J., Finkbeiner, D. P., & Davis, M. 1998, ApJ, 500, 525
Smith, D et al, 2010, MNRAS, in prep
Wang, L., & Rowan-Robinson, M. 2009, MNRAS, 398, 109